Geosci. Model Dev. Discuss., 8, 761–789, 2015
www.geosci-model-dev-discuss.net/8/761/2015/
doi:10.5194/gmdd-8-761-2015

Geoscientific Model Development Discussions
Open Access

An updated interparcel mixing algorithm in the Lagrangian advection scheme with shape matrix (LASM) v0.2

L. Dong[1], B. Wang[1,2], and L. Liu[2]

[1]LASG, Institute of Atmospheric Physics, Chinese Academy of Sciences, Beijing, China
[2]Ministry of Education Key Laboratory for Earth System Modelling, Center for Earth System Science (CESS), Tsinghua University, Beijing, China

Received: 3 January 2015 – Accepted: 19 January 2015 – Published: 30 January 2015

Correspondence to: L. Dong (dongli@lasg.iap.ac.cn)

Published by Copernicus Publications on behalf of the European Geosciences Union.

Abstract

The interparcel mixing algorithm in the Lagrangian advection scheme with shape matrix (LASM) is updated to make the scheme more robust. The linear degeneration criterion is replaced by the maximum deviation of the skeleton points so that the new algorithm is more effective in controlling the shape of parcels, which is vital for long time simulation. LASM is inherently shape-preserving without any complicated filter or limiter, so it is linear. This fact contributes to the ability of LASM of preserving the sum of multiple tracers exactly. A newly proposed terminator "toy"-chemistry test is also used to test LASM, which shows that LASM can preserve the weighted sum of two reactive chlorine-like species precisely.

1 Introduction

Lagrangian modeling approaches have long been recognized as a better alternative to the Eulerian or semi-Lagrangian ones for modeling the advection of tracers, due to their ability to reduce the numerical diffusion significantly, though some roadblocks need to be cleared. Therefore, more and more Lagrangian advection (or transport) schemes were proposed during the last two decades from different research communities. Based on the application objects, the research directions of the Lagrangian methods can be divided into four categories: (1) atmospheric dispersion modeling, (2) atmospheric chemical transport modeling, (3) cloud-resolving modeling, and (4) general circulation modeling. Lin et al. (2013) gave a panoramic view of the Lagrangian modeling of the atmosphere.

In the first category, the turbulent diffusion needs to be tackled thoroughly, because the temporal and spatial scales are relatively short and small respectively. These models are called Lagrangian Particle Dispersion Model (LPDM). The flow is decomposed into resolved mean and unresolved turbulent parts (the molecular diffusion is regularly ignored), where the first part comes from the reanalysis or model output, and the latter

GMDD
8, 761–789, 2015

part is described by the stochastic process (Thomson, 1987). Two of the representative schemes (or models) are HYSPLIT (Draxler and Hess, 1998) and FLEXPART (Stohl et al., 2005), which are used widely in the atmospheric emergency response, such as the volcanic ash cloud simulation. It is noteworthy that their turbulent diffusion formulations are different. Although the turbulent diffusion are both formulated in terms of the turbulent velocity components, FLEXPART solves the Langevin equation with the assumption of a Markov process, but HYSPLIT uses an autocorrelation coefficient and a random component. Recently, FLEXPART was extended to WRF in Brioude et al. (2013). Another model is NAME III developed in UK Met Office (Jones et al., 2007).

The Chemical Transport Models (CTM) consider a large number of tracer species and chemical reactions in the second category. One of the widely used Lagrangian CTMs is STOCHEM (Collins et al., 1997; Stevenson et al., 1997, 1998; Utembe et al., 2010). Chemical Lagrangian Model of the Stratosphere (CLaMS) (McKenna et al., 2002b, a) is a more sophisticated CTM with a featured flow deformation based interparcel mixing. Hoppe et al. (2014) implemented CLaMS into ECHAM/MESSy Atmospheric Chemistry model (EMAC), and compared it with the standard flux-form semi-Lagrangian (FFSL) transport scheme in EMAC. In their results, the transport barriers at the edge of the polar vortex are better simulated in CLaMS. Another Lagrangian CTM is CiTTyCAT (Pugh et al., 2012). The boundaries between the above two categories are actually blurred, for example STOCHEM is incorporated in NAME III.

The third category includes the works on the cloud simulation in Lagrangian way. The clouds are divided into warm clouds and ice clouds. Shima et al. (2009) proposed a named super-droplet method (SDM) aimed at warm clouds. Each super-droplet represents a multiple number of droplets with the same attributes and position. Sölch and Kärcher (2010) introduced a novel Lagrangian Cirrus Module (LCM), where the ice phase is simulated by a large number of simulation ice particles (SIPs). Compared with the tradition bulk and bin schemes that contain heavily parameterized microphysics and radiative processes, LCM has less numerical diffusion, and the simulated processes are more consistent without imposing thermodynamic equilibrium assumptions. Fur-

GMDD
8, 761–789, 2015

thermore, Unterstrasser and Sölch (2014) added SIP splitting and merging operations to increase the efficiency of LCM.

The fourth research effort comes from the general circulation modeling (GCM) community. The current research topic is the Lagrangian advection scheme in the dynamical core, that is to replace the Eulerian or semi-Lagrangian schemes by the Lagrangian ones. The turbulent diffusion is not considered, which is left to other physical parameterizations. The pioneer works were done by Reithmeier and Sausen (2002), which proposed Atmospheric Tracer Transport In a LAgrangian model (ATTILA). ATTILA was incorporated in ECHAM4 atmospheric GCM (AGCM) in Stenke et al. (2008), and positive results were gained compared with the standard semi-Lagrangian scheme, because ATTILA is able to maintain steeper and more realistic gradients. In Kaas et al. (2013), a hybrid Eulerian–Lagrangian scheme (HEL) was proposed, which has some similarities to particle in cell (PIC) methods. In HEL, one Eulerian scheme is running in parallel with the Lagrangian scheme, and their results are merged each time step. Lagrangian Advection scheme with Shape Matrix (LASM), which was proposed in Dong et al. (2014) and is the research object of this study, also belongs to this category. LASM conserves the tracer total mass strictly in the sense of parcels, which is similar to ATTILA. Stenke et al. (2009) used ATTILA in a fully coupled Chemistry–Climate Model (CCM), so the fourth category is also blurred with the second one, and may be even with the first one in the future to form a unified scheme.

The major roadblock of the Lagrangian schemes is the aliasing error, which manifests itself as noises in the tracer density distribution. During the advection, the discrete parcels (or called particles, mass packets in other works) are assumed to be isolated from each other. When the flow is nonlinearly deformative, the shape of parcels will be deformed or elongated into filaments, or even be split into parts. Most Lagrangian advection schemes do not explicitly simulate the parcel shape, and assume the parcel represents the mean state of a compact volume around it. This assumption of the parcel shape is generally not valid, so large aliasing error will occur when remapping the tracer density onto the mesh of a GCM, if no interparcel mixing is considered. Differ-

GMDD
8, 761–789, 2015

ent researchers designed different interparcel mixing algorithms to reduce or eliminate such errors. For example, ATTILA redefines the parcel boundaries by bringing the mass mixing ratio c of a species in a parcel closer to an average background mixing ratio, or called "interaction by exchange with mean", which is similar in STOCHEM (Stevenson et al., 1998). More advanced algorithms are devised in CLaMS that uses a Lyapunov exponent to measure for the deformation in the flow and inserts or merges parcels based on this exponent, and in HEL that incorporates the deformation rate of the flow and mixes tracers in a directionally biased way. Different from them, LASM explicitly describes the parcel shape by a linear deformation matrix, so a parcel can be rotated and stretched, not just translated. By doing this, the flow deformation plays an important role in the remapping process. Meanwhile an adaptive mixing algorithm incorporating the directionally biased idea in HEL is proposed, but it is not through the mesh. In summary, any successful Lagrangian scheme must has an effective interparcel mixing algorithm.

This work mainly updates the interparcel mixing algorithm in LASM (reported in Sect. 2.2) to make it more robust, and several tests are used to verify the performance of LASM in Sect. 3, including a new terminator "toy"-chemistry test (Lauritzen et al., 2014) for the CTMs (reported in Sect. 3.3). The conclusions are drawn in Sect. 4.

2 LASM details

The basic formulation of LASM (e.g., linear deformation matrix, skeleton points) was introduced in Dong et al. (2014), and only key ideas are restated below. The interparcel mixing algorithm is redesigned to overcome the potential problems in the old one.

2.1 Key ideas

The continuous fluid is discretized into parcels in finite number N_p. The centroids of parcels are $\{\boldsymbol{x}_{\mathbf{0}i}, i = 1, \ldots, N_p\}$. The shape of parcel i is approximated by a linear de-

GMDD
8, 761–789, 2015

formation matrix $\mathbf{H}_i$, so in 2-D cases, the parcels are represented as ellipses that can be translated, rotated and stretched. A spatial coordinate $\boldsymbol{x}$ can be transformed into a local coordinate system with $\boldsymbol{x}_{\mathbf{0}_i}$ as the origin:

$$\boldsymbol{x} = \boldsymbol{x}_{\mathbf{0}_i} + \mathbf{H}_i \boldsymbol{y}, \tag{1}$$

$$\boldsymbol{y} = \mathbf{H}_i^{-1} \left(\boldsymbol{x} - \boldsymbol{x}_{\mathbf{0}_i} \right), \tag{2}$$

where $\boldsymbol{y}$ is the local coordinate for $\boldsymbol{x}$. To avoid the problems caused by the poles on the sphere, the above calculation is currently transferred onto a local stereographic projection plane with $\boldsymbol{x}_{\mathbf{0}_i}$ still as the origin:

$$\widetilde{\boldsymbol{x}} = \mathbf{H}_i \boldsymbol{y}, \tag{3}$$

$$\boldsymbol{y} = \mathbf{H}_i^{-1} \widetilde{\boldsymbol{x}}, \tag{4}$$

where $\widetilde{\boldsymbol{x}}$ is the projected coordinate for $\boldsymbol{x}$. In 2-D cases, four skeleton points are associated with each parcel for sensing the deformation of the flow, and $\mathbf{H}_i$ is determined by those points. The SVD (singular value decomposition) technique is used to decompose $\mathbf{H}_i$ as

$$\mathbf{H}_i = \mathbf{U}_i \mathbf{S}_i \mathbf{V}_i, \tag{5}$$

where $\mathbf{S}_i$ is a positive diagonal scaling matrix with the diagonal elements in descending order, and $\mathbf{U}_i$ and $\mathbf{V}_i$ are matrices for rotation. The product of the diagonal elements of $\mathbf{S}_i$ is the determinant of $\mathbf{H}_i$.

The parcel i carries an amount of masses $\{m_i^s, s = 1, \ldots, N_s\}$ and densities $\{\rho_i^s, s = 1, \ldots, N_s\}$ for each tracer species. The centroid and densities of parcel i are updated by

$$\frac{\mathrm{d}\boldsymbol{x}_{\mathbf{0}i}}{\mathrm{d}t} = \boldsymbol{V}, \tag{6}$$

$$\frac{\mathrm{d}\rho_i^s}{\mathrm{d}t} = -\rho_i^s \nabla \cdot \boldsymbol{V}, s = 0, \ldots, N_s, \tag{7}$$

GMDD
8, 761–789, 2015

where $\boldsymbol{V}$ is normally the gridded velocity field from the external models or data. In this study, $\boldsymbol{V}$ is on the lat-lon mesh, and is interpolated onto the parcels by using bilinear interpolation.

The volume V_i of parcel i is defined by the first species:

$$V_i = \frac{m_i^0}{\rho_i^0}, \tag{8}$$

and it should be the same for other species. On the other hand, V_i should be equal to the determinant of $\mathbf{H}_i$. Generally, they are different, so the determinant of $\mathbf{H}_i$ is reset to V_i by scaling $\mathbf{S}_i$, and $\mathbf{H}_i$ is reconstructed from Eq. (5) each time step.

The anisotropic remapping between tracer parcels and the model grids is the same as in Dong et al. (2014), except for the global mass fixer on the mesh. The fixer is used to ensure that the total tracer mass on the grids is conserved, but it should be noted that the mass is already conserved exactly on the parcels in LASM, which is different from the traditional non-conservative semi-Lagrangian schemes. Therefore, it is arguable that the mass fixer can be dismissed in LASM. ATTILA in ECHAM4 (Reithmeier and Sausen, 2002) also does not consider the mass fixer. On the other hand, the mass fixer will sabotage the desired features of the Lagrangian schemes. For example, without the mass fixer, the constant sum of three discontinuous tracers in the deformation test case (Lauritzen and Thuburn, 2012) is exactly preserved in LASM (not shown), which is hardly achieved by the Eulerian and semi-Lagrangian schemes due to the use of nonlinear shape-preserving filters, but when using mass fixer, this feature is lost in LASM, although the error is much smaller.

By now, the trajectories and densities of parcels are calculated, and the densities are remapped onto the grids. The next important ingredient of LASM is the interparcel mixing algorithm, which is updated as follows.

GMDD
8, 761–789, 2015

2.2 Interparcel mixing

Due to the discretization of the continuous fluid, an initial compact parcel cannot keep its integrity under the deformation of the flow. Some part of it needs to be exchanged with other parcels to form some kind of interparcel mixing, which will improve the degree of linear approximation of the parcel shape.

Previously, a parcel with index i is judged to be mixed or not according to a disorder degree $\mathcal{D}_i$, which is the ratio between the maximum and mean angles between the major axes of the parcel and its surrounding or neighbor parcels. When $\mathcal{D}_i$ is greater than a given threshold, the parcel i is mixed with its neighbors by distributing tracer masses to them, and its major axis is shrunk by a fixed factor 0.05. The volumes of the neighbor parcels are increased accordingly. $\mathcal{D}_i$ is a good indicator of the flow condition, but this criterion and mixing manner failed in some cases, and caused extremely large and small parcels to exist in a barotropic test case. In this study, a more effective criterion and mixing manner are designed to better control the shape of parcels. A transition function

$$f(x_0, y_0, x_1, y_1, x) = \begin{cases} y_0 & x \le x_0 \\ (y_1 - y_0)(4 - 3t)t^3 + d_0 & x_0 < x \le x_1 \\ y_1 & x > x_1 \end{cases}, t = \frac{x - x_0}{x_1 - x_0} \tag{9}$$

is used to construct some thresholds.

The parcel shape is approximated by a linear deformation matrix $\mathbf{H}_i$ as aforementioned. When the flow is linearly or quasi-linearly deformative, or the sizes of parcels are small enough compared with the deformation scale, this approximation is sufficient so that the parcels are free to sense the flow deformation. Meanwhile, the ratio between the major and minor axis length γ_i is limited to a maximum value γ_m to keep the parcel compact, because long parcels will cause extensive computation for searching connected grids. Otherwise the linear approximation may quickly degenerate, and this causes poor remapping, since the parcel shapes are not well simulated. The most

GMDD
8, 761–789, 2015

direct symptom of this degeneration is that the positions of skeleton points (say $\boldsymbol{s}$) deviate from the ones calculated from $\mathbf{H}_i$ (say $\boldsymbol{s}'$), see Fig. 1 for an example. The deviation is calculated by

$$d = \frac{D(\boldsymbol{s}, \boldsymbol{s}')}{L}, \tag{10}$$

where function $D(.,.)$ is the spherical distance on the sphere, and L is the half length of the major axis of the parcel. By defining in this way, d is a dimensionless number, and independent on the underlying domain (e.g., Earth radius). When the maximum deviation $d_{\max}$ of the skeleton points is greater than a given threshold d^*, $\mathbf{H}_i$ is not regarded as a good approximation to the real shape of parcel i. The threshold is determined by

$$d^* = f(r_0, d_0, r_1, d_1, r), r = r_{\mathrm{v}i}\gamma_i, \tag{11}$$

where d_0 (0.5) and d_1 (0.1) are the looser and stricter thresholds, r_0 (1) and r_1 (5) are the transition range, $r_{\mathrm{v}i}$ is the ratio between the volume of parcel i and the mean volume of it and its neighbors. In summary, the more elongated and larger parcel will have a stricter threshold.

Another difference from the old mixing algorithm is that the neighbor parcel shapes are not changed, so those parcels will not be disturbed by the mixing. The parcel i is not simply shrunk, and its volume is kept unchanged. The tracer density of the parcels is changed in the following manner, which is similar with the ones used in Stevenson et al. (1998) and Reithmeier and Sausen (2002), but it is not through the mesh, and respects the local flow properties. Note the tracer species index is omitted for simplicity. Firstly, a weight w_j for the neighbor parcel j is calculated as before (see Eq. 18 in Dong et al., 2014), and the parcel i has a unit weight. The neighbor parcel that is closer to the parcel i along the major axis has a larger weight, so the weight is directionally biased as HEL. Then the mean density of parcels weighted by w_j is

$$\overline{\rho}_i = \frac{1}{\sum_{k\in\mathcal{S}_i} w_k V_k} \sum_{j\in\mathcal{S}_i} w_j m_j, \tag{12}$$

GMDD
8, 761–789, 2015

where m and V are the mass and volume respectively, S_i is the parcel index set of parcel i and its neighbors. The density of each neighbor parcel is restored to $\overline{\rho}_i$ as

$$\rho_j^* = \rho_j + C_{mj}\left(\overline{\rho}_i - \rho_j\right), \tag{13}$$

where $C_{mj} = w_j C_m$, and C_m is a restore coefficient that controls the mixing degree. C_m should be related to the time step size. It can also be variant along the vertical direction. The density of parcel i is calculated under the constraint of mass conservation as

$$\begin{aligned}\rho_i^* &= \frac{M_i - \sum_{j\in S_i, j\neq i}\rho_j^* V_j}{V_i} \\ &= \rho_i + C_m\left(\overline{\rho}_i - \rho_i\right).\end{aligned} \tag{14}$$

It can be seen that the parcel i is just restored to $\overline{\rho}_i$ with the coefficient C_m, and the mass on the parcels is exactly conserved during the mixing.

After the density mixing calculation, the shape of parcel i is changed through reducing γ_i. In 2-D cases,

$$\text{Before mixing: } \frac{S_0}{S_1} = \gamma_i, S_0 S_1 = V_i, \tag{15}$$

$$\text{After mixing: } \frac{S_0^*}{S_1^*} = \alpha\gamma_i, S_0^* S_1^* = V_i, \tag{16}$$

where S_0 and S_1 are the diagonal elements of $\mathbf{S}_i$, α is a reduction factor, and is determined by

$$\alpha = f(\gamma_0, \alpha_0, \gamma_1, \alpha_1, \gamma_i), \tag{17}$$

GMDD
8, 761–789, 2015

where $\gamma_0 = 1$, $\alpha_0 = 1$, $\gamma_1 = 5$ and $\alpha_1 = 0.5$. This setup will make the shape of parcel i closer to circle in 2-D cases. After some simple manipulation,

$$S_0^* = \sqrt{\alpha} S_0, \tag{18}$$

$$S_1^* = \frac{1}{\sqrt{\alpha}} S_1. \tag{19}$$

Then the deformation matrix $\mathbf{H}_i$ is updated, and the skeleton points are reset accordingly.

The mixing in the Lagrangian schemes is driven by the flow deformation, whereas the inherent mixing in the Eulerian and semi-Lagrangian schemes is driven by the tracer density gradient, which is similar to the molecular diffusion. Currently, the above interparcel mixing is only for the computational aspect, but when the physical mixing is required, the similar form can be utilized with different parameters (Stevenson et al., 1998). For example, the disorder degree $\mathcal{D}_i$ can be used as a trigger of the turbulent mixing. In addition, the stochastic turbulent diffusion in LPDM may be incorporated in the future to unify them.

2.3 Tendency evaluation

In the real applications, some other processes will calculate the tendencies for different tracer species. There are two types of tendency in LASM. The tendency in the first type resides on the Eulerian mesh of an existing model, such as the physics parameterizations (e.g., convection, microphysics) in an AGCM. The gridded tendencies need to be remapped onto the parcels, and the remapping formula is the same as the one for the tracer density in LASM. In other Lagrangian schemes, the tendency on a mesh cell is distributed evenly to each parcel contained in that cell (Stevenson et al., 1998; Reithmeier and Sausen, 2002). The tendency in the second type is computed directly on the parcels, which is more natural, such as the chemical reactions in a CTM.

For the applications in an AGCM, only the first type tendency can be used currently, since the mainstream physics parameterizations are all defined on the vertical columns

GMDD
8, 761–789, 2015

of the mesh, for example ATTILA in ECHAM4 (Stenke et al., 2008). Nevertheless, there are some researches (Shima et al., 2009; Andrejczuk et al., 2010; Sölch and Kärcher, 2010; Unterstrasser and Sölch, 2014) on the microphysics, which constructed numerical schemes to simulate cloud and precipitation in the Lagrangian framework. In the CTMs, it is easier to compute the tendencies, because the chemical reactions take place on the parcels. Several Lagrangian CTMs exist, such as STOCHEM, CLaMS (McKenna et al., 2002a), etc., but NAME III calculates the chemistry on a fixed three-dimensional chemistry grid (Jones et al., 2007). Grewe et al. (2014) also investigated how the tendency should be evaluated.

The two types of the tendency are both implemented in LASM, and their influence on the simulation results of a newly proposed test case with chemical reactions is shown in Sect. 3.3.

2.4 Roadmap of LASM

Although LASM is a numerical scheme, it will be beneficial to do strict version control on its implementation following the software engineering practices. The following list is the future roadmap of LASM. More features will be added step by step.

v1.0 Application in an AGCM in 2.5-D mode with the vertical formulation unchanged.

v1.1 Parallel acceleration with the help of OpenMP and MPI.

v1.* Handle the horizontal boundaries for application in an OGCM.

v2.0 Fully 3-D setup with different vertical coordinates.

v2.* Application in an CTM.

v3.0 Incorporate dynamics into 2-D LASM to form a barotropic dynamical core.

v4.0 Incorporate dynamics into 3-D LASM to form a baroclinic dynamical core.

v5.0 Incorporate stochastic processes to form a dispersion model.

GMDD
8, 761–789, 2015

3 Test cases

In this section, three test cases are used to verify the modifications of LASM. The first two cases are the same as used in Dong et al. (2014). The third one is newly proposed in Lauritzen et al. (2014), which extends the previous inert scalars to reactive species.

3.1 Deformation flow test

The deformation flow test was first proposed in Nair and Lauritzen (2010), and further extended in Lauritzen et al. (2012), which contains four large scale deformation flow formulas to challenge the advection schemes. In this study, we repeat the case with non-divergent flow to test the basic performance of the new interparcel mixing algorithm. The spatial resolution of the mesh is $1.5^\circ \times 1.5^\circ$, and the normalized flow period T is 5.

The effects of changing γ_m are shown in Fig. 2, which shows the mixing ratio distribution of the slotted cylinders at $t = T/2$ and $t = T$, and in Table 1, which lists the correlation diagnostics with and without mass fixer. With the decreasing of γ_m, the parcels, which are under heavily stretching and shearing, cannot turn to be too long, and their tracer masses will be mixed with the neighbor parcels. When $\gamma_m = 2$, the filament structures of the slotted cylinders break up at $t = T/2$. This resembles the aliasing error shown in Fig. 13 in Dong and Wang (2012), and in Fig. 7 in Kaas et al. (2013). As expected, the real mixing diagnostics I_r is also larger when γ_m is small. In spite of this, it does not mean γ_m should be as large as possible. For example, in the following terminator "toy"-chemistry test, when the tendencies for the tracers are considered, the larger γ_m causes the burr edge along the terminator as shown in Fig. 7. Therefore, the moderate value 5 for γ_m is used in LASM. By comparing Fig. 2 (the third row with $\gamma_m = 10$) with Fig. 12 in Dong et al. (2014) (the third row), it can be seen that the new algorithm is a little better to keep the final shape of the slotted cylinders, and I_r is 1.59×10^{-4} in the new algorithm, which is 3.54×10^{-4} in the old one.

GMDD
8, 761–789, 2015

Another observation from Table 1 is that: when the mass fixer on the grids is used, the unmixing and overshooting diagnostics (l_u and l_o) are not all zero. Therefore, we turn off the mass fixer, because the tracer total mass is already conserved on the parcels, and the mass fixer causes the losing of desired features (e.g., linear, shape-preserving) in LASM.

The effects of changing C_m are shown in Fig. 3. By increasing C_m, the mixing degree is enlarged, especially when $C_m = 0.1$. In the current study, the value 0.001 is chosen, which is the same as STOCHEM and ATTILA.

3.2 Barotropic test

The barotropic test provides more realistic flow, though no analytical solution is available. The same finite difference barotropic model is used to drive LASM. The spatial resolution is $1.5^\circ \times 1.5^\circ$, and the time step size is 20 s to ensure the stability of the model. The initial conditions and topography are as subcase 2 in Dong et al. (2014).

Firstly, we check the validity of the new criterion that judges the linear degeneration. The comparison between the old and new criterion is shown in Fig. 4. In the old one, many extremely large and small parcels appear, but they are eliminated in the new one. Therefore, the new criterion is better, and should replace the old one. Secondly, two triggers for the interparcel mixing are compared. The first one is *minimum mixing*, that is the linear degeneration of the parcel shape triggers the mixing. The second one is *all mixing*, that is the mixing is active each time step for each parcel, but only the shapes of the degenerated parcels are changed. The results at day 4 are in Fig. 5. Clearly, all mixing causes substantial diffusion than minimum mixing. Based on this comparison, LASM manifests its ability of customizable mixing, and more physics-based triggers can be devised with the information available in LASM to fulfill different needs.

GMDD
8, 761–789, 2015

3.3 Terminator "toy"-chemistry test

This test (Lauritzen et al., 2014) consists of transporting two reacting chlorine-like species (Cl and Cl_2) in the deformation flow. Although the chemical reactions are non-linear, the weighted sum $Cl_y = Cl + 2Cl_2$ (i.e., linear correlation) is preserved, even when the reactions are discretized. In addition, one of the reactions ($Cl_2 \xrightarrow{k_1} 2Cl$) is photolytic so that the reaction rate k_1 is terminator-"like" and will produce very steep gradients in the chlorine species near the terminator. Only the schemes that are semi-linear can preserve the linear tracer correlation (i.e., Cl_y). Many Eulerian or semi-Lagrangian schemes satisfy the semi-linear constraint when the shape-preserving filters are not applied, but in the real cases, such schemes must be limited by the filters to avoid adverse oscillations that may cause instability, so the linear correlation between the two species is lost. On the other hand, the Lagrangian schemes have the intrinsic property of being linear, so no complicated (maybe nonlinear) filter or limiter is needed to ensure the monotonicity. The linear property is the sufficient condition for the semi-linear property (Lauritzen and Thuburn, 2012). For example, LASM can preserve the constant sum of three tracers, which is more challenging than two tracers.

Except the scheme itself, the tendency evaluation and physics-dynamics coupling types also affect the results. In LASM, the tendencies of Cl and Cl_2 are evaluated on the parcels and grids respectively. The spatial resolution of the lat-lon mesh is $1^\circ \times 1^\circ$. The time step size Δt is 1800s both for the chemistry and advection processes, because there is no need to use a smaller Δt in LASM, so the physics-dynamics coupling type is as ftype = 1 in Lauritzen et al. (2014). The results for Cl, Cl_2 and Cl_y at day 6 are shown in Fig. 6. Firstly, the constant Cl_y is preserved exactly in both cases. The results of CAM-FV and CAM-SE can be referred in Fig. 3 in Lauritzen et al. (2014), which indicates that Cl_y is disturbed in those schemes caused by the used shape-preserving filters. Secondly, it is obvious that the results with the tendencies evaluated on the parcels (i.e., the chemical reactions occur on the parcels) are better. In Fig. 8, the cross sections of Cl and Cl_2 at 45° S exhibit that LASM is shape-preserving inherently

GMDD
8, 761–789, 2015

without any complicated and nonlinear filter, and the sharp gradients are simulated well near the terminator. By contrast, CAM-SE shows Gibbs phenomena when no filter or limiter is used (see Fig. 5 in Lauritzen et al., 2014).

4 Conclusions

The interparcel mixing algorithm in LASM is updated through replacing the criterion of the linear degeneration of the parcel shape and the mixing manner. The new criterion is a more direct indicator for the degeneration symptom, so the parcel shape is better controlled. In the new mixing manner, the restore coefficient C_m is used to adjust the mixing degree. Several tests are utilized to verify the updates, including a newly proposed terminator "toy"-chemistry test. The results reveal that the new algorithm is effective and less arbitrary. It is noteworthy that LASM is a linear scheme, so it can preserve the sum of multiple tracer species and also the weighted sum of two reactive chlorine-like species exactly. Two triggers for the interparcel mixing are compared, and LASM shows the great flexibility so that different triggers can be devised in the future to address different needs.

Code availability

The codes of LASM are managed by using GIT and hosted in GitHub. The repository URL is https://github.com/dongli/LASM. There are also two repositories, GEOMTK (https://github.com/dongli/geomtk) and BARAOTROPIC-MODEL (https://github.com/dongli/barotropic-model), used by LASM as submodules. You can download all of them by invoking the following command in a shell:

```
$ git clone --recursive https://github.com/dongli/LASM
```


GMDD
8, 761–789, 2015

Four external libraries (Boost, Armadillo, NetCDF and MLPACK) are also needed to be installed. You can install them by using a package manager called PACKMAN (https://github.com/dongli/packman) developed by the authors.

The Supplement related to this article is available online at doi:10.5194/gmdd-8-761-2015-supplement.

Acknowledgements. This work is supported by the National Natural Science Foundation of China (grant no. 41305094) and the National Grand Fundamental Research 973 Program of China (grant no. 2014CB441302).

References

Andrejczuk, M., Grabowski, W. W., Reisner, J., and Gadian, A.: Cloud-aerosol interactions for boundary layer stratocumulus in the Lagrangian Cloud Model, J. Geophys. Res., 115, D22214, doi:10.1029/2010JD014248, 2010. 772

Brioude, J., Arnold, D., Stohl, A., Cassiani, M., Morton, D., Seibert, P., Angevine, W., Evan, S., Dingwell, A., Fast, J. D., Easter, R. C., Pisso, I., Burkhart, J., and Wotawa, G.: The Lagrangian particle dispersion model FLEXPART-WRF version 3.1, Geosci. Model Dev., 6, 1889–1904, doi:10.5194/gmd-6-1889-2013, 2013. 763

Collins, W. J., Stevenson, D. S., Johnson, C. E., and Derwent, R. G.: Tropospheric ozone in a global-scale three-dimensional Lagrangian model and its response to NO_x emission controls, J. Atmos. Chem., 26, 223–274, 1997. 763

Dong, L. and Wang, B.: Trajectory-tracking scheme in Lagrangian form for solving linear advection problems: preliminary tests, Mon. Weather Rev., 140, 650–663, 2012. 773

Dong, L., Wang, B., and Liu, L.: A Lagrangian advection scheme with shape matrix (LASM) for solving advection problems, Geosci. Model Dev., 7, 2951–2968, doi:10.5194/gmd-7-2951-2014, 2014. 764, 765, 767, 769, 773, 774

Draxler, R. R. and Hess, G. D.: An overview of the HYSPLIT4 modelling system for trajectories, dispersion, and deposition, Aust. Meteorol. Mag., 47, 295–308, 1998. 763

GMDD
8, 761–789, 2015

Grewe, V., Brinkop, S., Jöckel, P., Reich, S. S. S., and Yserentant, H.: On the theory of mass conserving transformations for Lagrangian methods in 3D atmosphere-chemistry models, Meteorol. Z., 23, 441–447, doi:10.1127/0941-2948/2014/0552, 2014. 772

Hoppe, C. M., Hoffmann, L., Konopka, P., Grooß, J.-U., Ploeger, F., Günther, G., Jöckel, P., and Müller, R.: The implementation of the CLaMS Lagrangian transport core into the chemistry climate model EMAC 2.40.1: application on age of air and transport of long-lived trace species, Geosci. Model Dev., 7, 2639–2651, doi:10.5194/gmd-7-2639-2014, 2014. 763

Jones, A. R., Thomson, D. J., Hort, M., and Devenish, B.: The UK Met Office's next-generation atmospheric dispersion model, NAME III, in: Air Pollution Modeling and its Application XVII Proceedings of the 27th NATO/CCMS International Technical Meeting on Air Pollution Modelling and its Application), edited by: Borrego, C. and Norman, A.-L., Springer, 580–589, 2007. 763, 772

Kaas, E., Sørensen, B., Lauritzen, P. H., and Hansen, A. B.: A hybrid Eulerian–Lagrangian numerical scheme for solving prognostic equations in fluid dynamics, Geosci. Model Dev., 6, 2023–2047, doi:10.5194/gmd-6-2023-2013, 2013. 764, 773

Lauritzen, P. H. and Thuburn, J.: Evaluating advection/transport schemes using interrelated tracers, scatter plots and numerical mixing diagnostics, Q. J. Roy. Meteor. Soc., 138, 906–918, 2012. 767, 775

Lauritzen, P. H., Skamarock, W. C., Prather, M. J., and Taylor, M. A.: A standard test case suite for two-dimensional linear transport on the sphere, Geosci. Model Dev., 5, 887–901, doi:10.5194/gmd-5-887-2012, 2012. 773

Lauritzen, P. H., Conley, A. J., Lamarque, J.-F., Vitt, F., and Taylor, M. A.: The terminator "toy"-chemistry test: a simple tool to assess errors in transport schemes, Geosci. Model Dev. Discuss., 7, 8769–8804, doi:10.5194/gmdd-7-8769-2014, 2014. 765, 773, 775, 776

Lin, J. C., Brunner, D., Gerbig, C., Stohl, A., Luchar, A., and Webley, P. (Eds.): Lagrangian Modeling of the Atmosphere, Geophysical Monograph Series, Vol. 200, American Geophysical Union, 2013. 762

McKenna, D. S., Grooß, J.-U., Günther, G., Konopka, P., and Müller, R.: A new Chemical Lagrangian Model of the Stratosphere (CLaMS) 2. Formulation of chemistry scheme and initialization, J. Geophys. Res., 107, ACH15.1–ACH15.15, doi:10.1029/2000JD000114, 2002a. 763, 772

McKenna, D. S., Konopka, P., Grooß, J.-U., Günther, G., Müller, R., Spang, R., Offermann, D., and Orsolini, Y.: A new chemical Lagrangian model of the stratosphere (CLaMS) 1. For-

GMDD
8, 761–789, 2015

mulation of advection and mixing, J. Geophys. Res. Atmos., 107, ACH4.1–ACH4.14, doi:10.1029/2000JD000113, 2002b. 763

Nair, R. D. and Lauritzen, P. H.: A class of deformational flow test cases for linear transport problems on the sphere, J. Comput. Phys., 229, 8868–8887, 2010. 773

Pugh, T. A. M., Cain, M., Methven, J., Wild, O., Arnold, S. R., Real, E., Law, K. S., Emmerson, K. M., Owen, S. M., Pyle, J. A., Hewitt, C. N., and MacKenzie, A. R.: A Lagrangian model of air-mass photochemistry and mixing using a trajectory ensemble: the Cambridge Tropospheric Trajectory model of Chemistry And Transport (CiTTyCAT) version 4.2, Geosci. Model Dev., 5, 193–221, doi:10.5194/gmd-5-193-2012, 2012. 763

Reithmeier, C. and Sausen, C.: ATTILA: atmospheric tracer transport in a Lagrangian model, Tellus B, 54, 278–299, 2002. 764, 767, 769, 771

Shima, S., Kusano, K., Kawano, A., Sugiyama, T., and Kawahara, S.: Ther super-droplet method for the numerical simulation of clouds and precipitation: a particle-based and probabilistic microphysics model coupled with a non-hydrostatic model, Q. J. Roy. Meteor. Soc., 135, 1307–1320, 2009. 763, 772

Sölch, I., and Kärcher, B.: A large-eddy model for cirrus clouds with explicit aerosol and ice microphysics and Lagrangian ice particle tracking, Q. J. Roy. Meteor. Soc., 136, 2074–2093, 2010. 763, 772

Stenke, A., Grewe, V., and Ponater, M.: Lagrangian transport of water vapor and cloud water in the ECHAM4 GCM and its impact on the cold bias, Clim. Dynam., 31, 491–506, 2008. 764, 772

Stenke, A., Dameris, M., Grewe, V., and Garny, H.: Implications of Lagrangian transport for simulations with a coupled chemistry-climate model, Atmos. Chem. Phys., 9, 5489–5504, doi:10.5194/acp-9-5489-2009, 2009. 764

Stevenson, D. S., Collins, W. J., Johnson, C. E., and Derwent, R. G.: The impact of aircraft nitrogen oxide emissions on tropospheric ozone studied with a 3D Lagrangian model including fully diurnal chemistry, Atmos. Environ., 31, 1837–1850, 1997. 763

Stevenson, D. S., Collins, W. J., Johnson, C. E., and Derwent, R. G.: Intercomparison and evaluation of atmospheric transport in a Lagrangian model (STOCHEM), and an Eulerian model (UM), using Rn as a short-lived tracer, Q. J. Roy. Meteor. Soc., 124, 2477–2491, 1998. 763, 765, 769, 771

GMDD
8, 761–789, 2015

Stohl, A., Forster, C., Frank, A., Seibert, P., and Wotawa, G.: Technical note: The Lagrangian particle dispersion model FLEXPART version 6.2, Atmos. Chem. Phys., 5, 2461–2474, doi:10.5194/acp-5-2461-2005, 2005. 763

Thomson, D. J.: Criteria fro the selection of stochastic models of particle trajectories in turbulent flows, J. Fluid Mech., 180, 529–556, 1987. 763

Unterstrasser, S. and Sölch, I.: Optimisation of the simulation particle number in a Lagrangian ice microphysical model, Geosci. Model Dev., 7, 695–709, doi:10.5194/gmd-7-695-2014, 2014. 764, 772

Utembe, S. R., Cooke, M. C., Archibald, A. T., Jenkin, M. E., Derwent, R. G., and Shallcross, D. E.: Using a reduced Common Representative Intermediates (CRIv2-R5) mechanism to simulate tropospheric ozone in a 3-D Lagrangian chemistry transport model, Atmos. Environ., 44, 1609–1622, 2010. 763

GMDD
8, 761–789, 2015

Table 1. The correlation results with and without mass fixer for different values of γ_m in the deformation test case 4.

	without mass fixer			with mass fixer		
γ_m	l_r	l_u	l_o	l_r	l_u	l_o
2	4.65×10^{-4}	0	0	5.36×10^{-4}	4.22×10^{-6}	5.22×10^{-4}
5	2.50×10^{-4}	0	0	2.60×10^{-4}	1.01×10^{-6}	9.89×10^{-5}
10	1.59×10^{-4}	0	0	1.62×10^{-4}	5.31×10^{-8}	0
100	1.20×10^{-4}	0	0	1.19×10^{-4}	2.56×10^{-8}	0

GMDD
8, 761–789, 2015

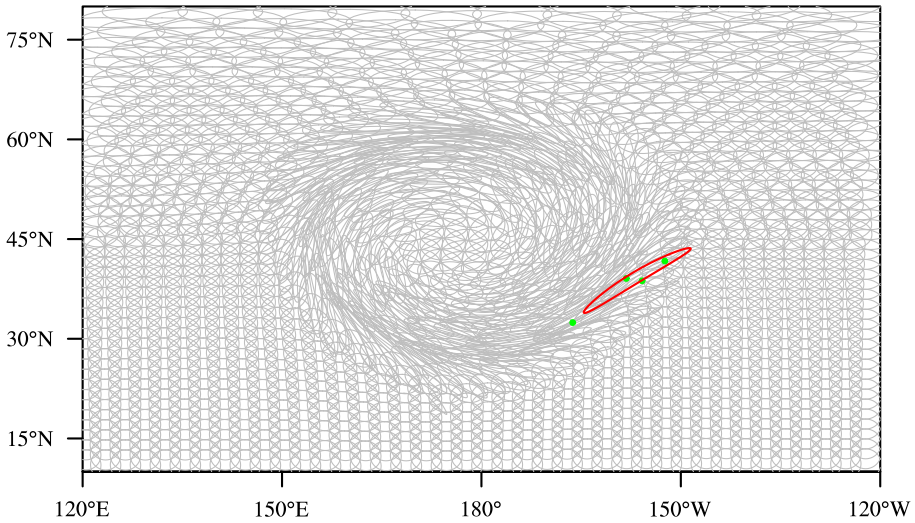

Figure 1. A case of linear approximation degeneration of a parcel. The red ellipse is the current shape of the parcel, and the green points are the skeleton points of the parcel.

GMDD
8, 761–789, 2015

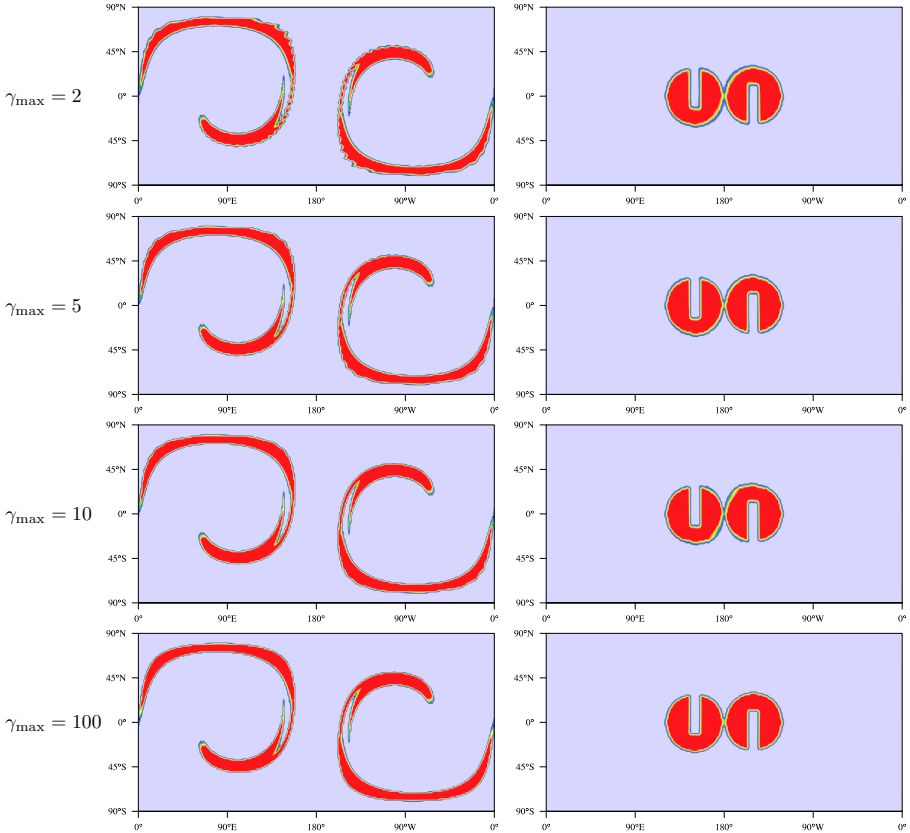

Figure 2. Deformation test case results with different γ_m. The left column is the slotted cylinders at $t = T/2$, and the right column is at $t = T$.

GMDD
8, 761–789, 2015

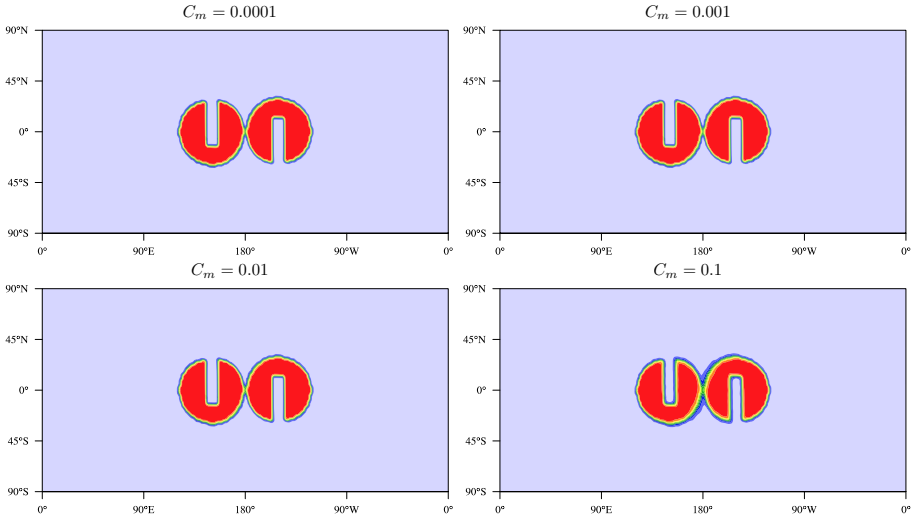

Figure 3. Deformation test case results with different C_m at $t = T$.

GMDD
8, 761–789, 2015

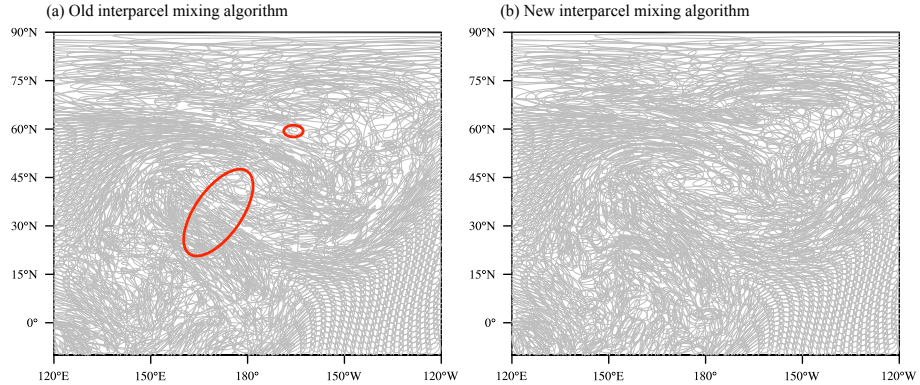

Figure 4. Comparison of the parcel shapes between the old and new interparcel mixing algorithms in a barotropic test case. Two extremely small and large parcels in the old algorithm are spotted by the red ellipses.

GMDD
8, 761–789, 2015

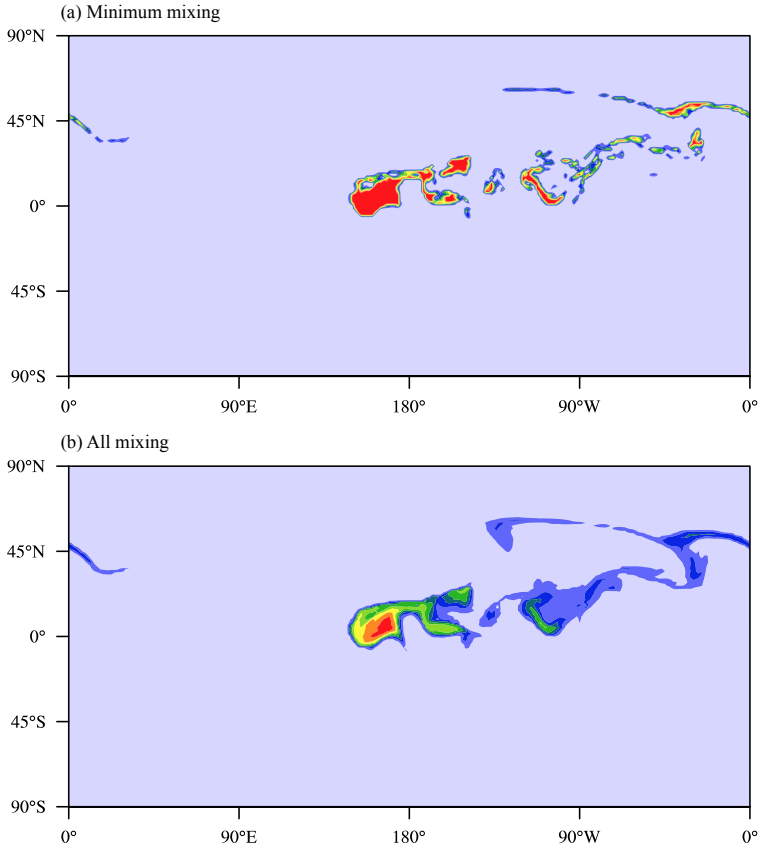

Figure 5. Comparison between minimum mixing and all mixing at day 4. All mixing means the interparcel mixing is triggered each time step for each parcel.

GMDD
8, 761–789, 2015

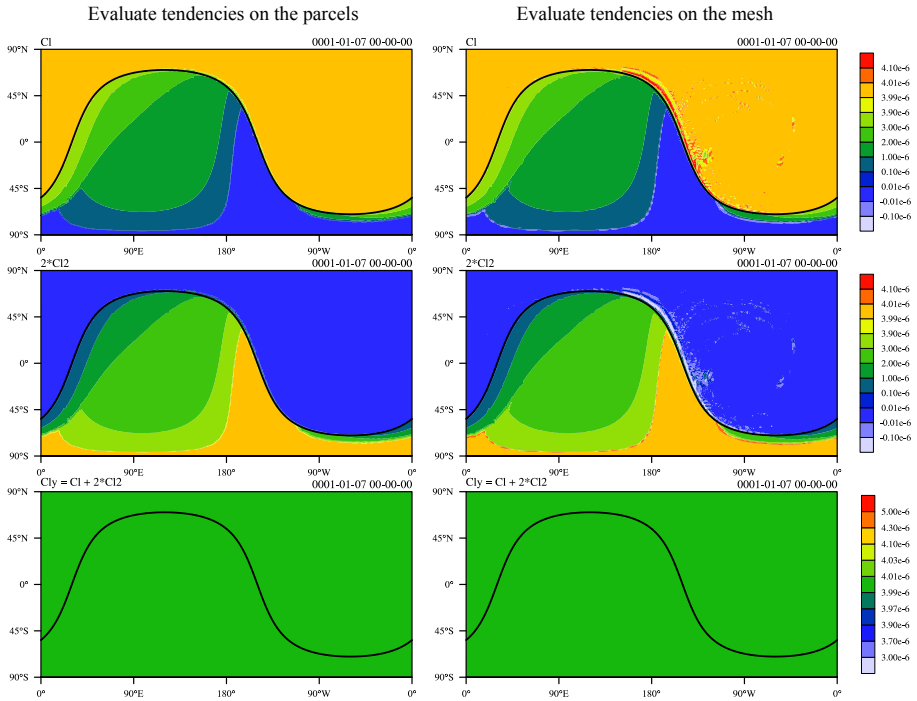

Figure 6. Contour plots of Cl, Cl_2 and Cl_y at day 6 for two types of tendency respectively. Solid black line is the location of the terminator line.

GMDD
8, 761–789, 2015

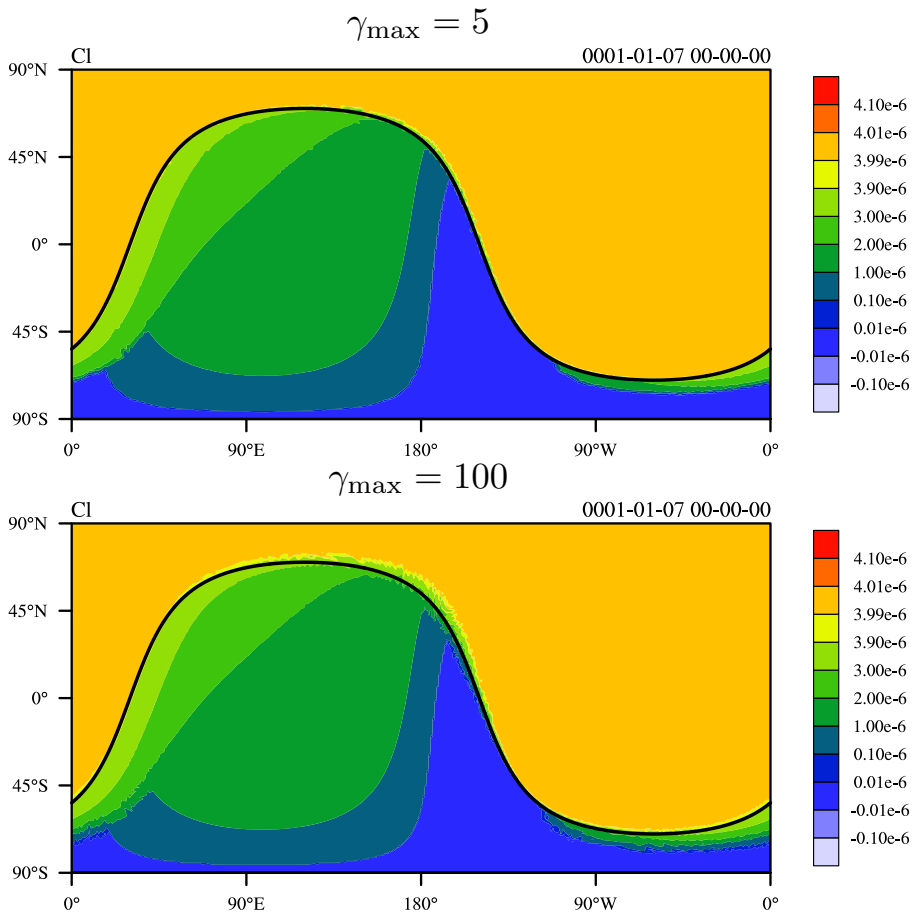

Figure 7. Contour plots of Cl at day 6 for two values of γ_m respectively. Solid black line is the location of the terminator line.

GMDD
8, 761–789, 2015

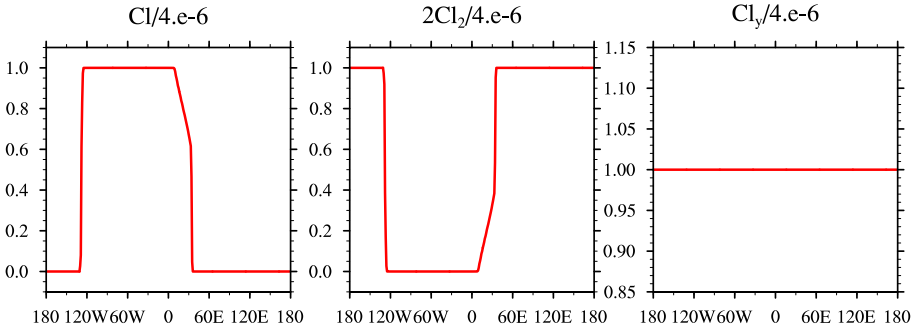

Figure 8. Cross section of Cl, Cl_2, and Cl_y at day 1. Results are normalized by 4×10^{-4} (the initial value of Cl_y.

GMDD
8, 761–789, 2015